Astrophys Space Sci (2009) 322: 195–199
DOI 10.1007/s10509-009-9997-6

ORIGINAL ARTICLE

Penetration of plasma across a magnetic field

C. Plechaty · R. Presura · S. Wright · S. Neff · A. Haboub

Received: 15 June 2008 / Accepted: 30 January 2009 / Published online: 14 February 2009

Abstract Experiments were performed at the Nevada Terawatt Facility to investigate the plasma penetration across an externally applied magnetic field. In experiment, a short-pulse laser ablates a polyethylene laser target, producing a plasma which interacts with an external magnetic field. The mechanism which allows the plasma to penetrate the applied magnetic field in experiment will be discussed.

Keywords Plasma penetration · Strong magnetic field · Laser plasma · Laboratory astrophysics · Instabilities · Magnetic Rayleigh-Taylor instability · Electromagnetic flute instability

1 Introduction

The plasmas considered in this paper are sufficiently conductive to affect the topology of the magnetic field. The mechanism which allows such a plasma to penetrate through a magnetic field is an important topic of study with a wide variety of applications, for example the interaction of the solar wind with the Earth's magnetic field. Several explanations exist for the mechanism which allows the solar wind to penetrate the Earth's magnetosphere. Some of these explanations include: magnetic reconnection (Dungey 1961), diffusion (Axford and Hines 1961), impulsive penetration (most recently reviewed in Echim and Lemaire 2000), and Rayleigh-Taylor instabilities of the magnetopause (Gratton et al. 1996).

The role of instabilities in the plasma penetration across a magnetic field was investigated in the laboratory at the Nevada Terawatt Facility (NTF). The interaction of a plasma flow (produced by ablating a polyethylene target with a short-pulse laser) with an external magnetic field (created by a pulsed-power generator) was investigated. In Sect. 2, the experiment will be presented. In Sect. 3, the magneto-hydrodynamic simulations performed to estimate some of the plasma parameters in experiment will be described. In Sect. 4 the role of instabilities in the plasma penetration will be discussed.

2 Experiment

An experiment was performed to investigate the interaction of a laser-produced plasma with an external magnetic field created by a pulsed power generator. A schematic of the experiment setup is shown in Fig. 1. A current pulse rising to 0.6 MA in 200 ns was driven by a 2 TW pulsed power generator through a cylindrical electrode to produce an azimuthal magnetic field. A polyethylene laser target was placed at 5–7 mm from the surface of the electrode, where the field

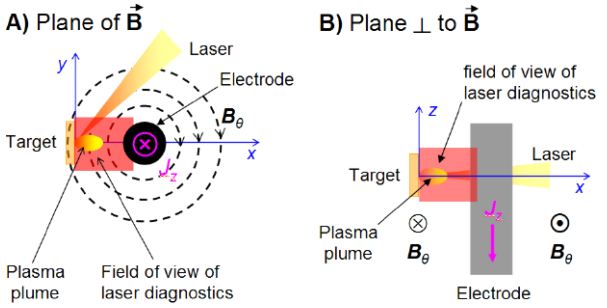

Fig. 1 Experimental setup used in Zebra, as viewed (**A**) in the plane parallel to the magnetic field, (**B**) in the plane perpendicular to the magnetic field

C. Plechaty (✉) · R. Presura · S. Wright · S. Neff · A. Haboub
Nevada Terawatt Facility, University of Nevada, Reno, USA
e-mail: plechaty@physics.unr.edu

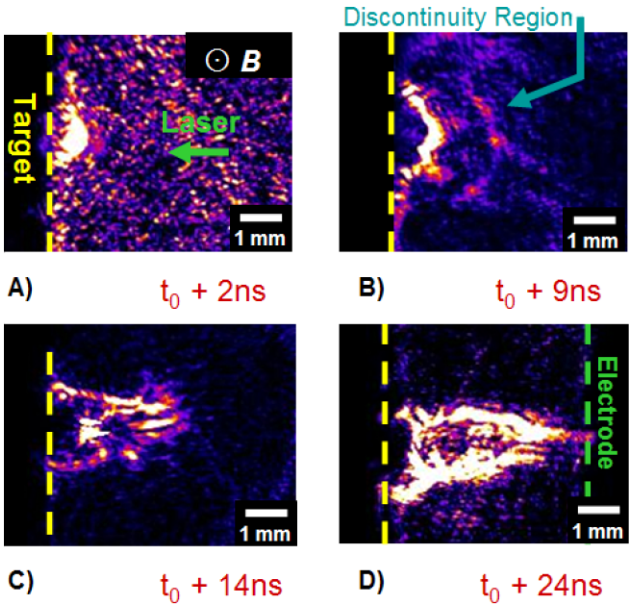

Fig. 2 Schlieren images taken in the plane perpendicular to the magnetic field. The ablation laser hits the target at the moment t_0. (**A**) Initially, the plasma expands hemi-spherically. (**B**) As the plasma is decelerated by the magnetic field, the density distribution shows the formation of a discontinuity region. (**C**) The plasma boundary becomes unstable. (**D**) Plasma penetrates the field. Frames **A** and **B** were obtained in the same shot, while **C** and **D** were obtained in different shots. Lighter areas denote larger plasma gradients

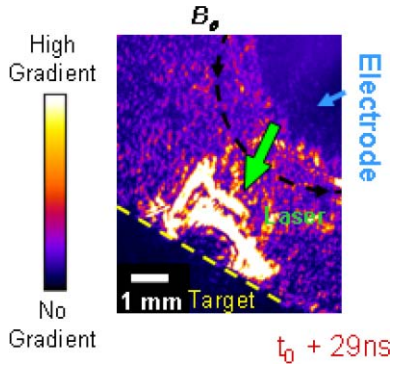

Fig. 3 Schlieren image taken in the plane of the magnetic field

strength was up to 17 T. The target was ablated by a 5 ps laser pulse with 2–4 J and irradiance up to 10^{16} W/cm^2. Since the laser pulse duration was much shorter than the plasma evolution time, in the absence of a magnetic field the plasma expanded quasi-adiabatically.

A variety of diagnostics were used in this experiment. The magnetic field in vacuum was measured with inductive probes (B-dot). The laser-produced plasma was observed with diagnostics based on the plasma refractive index. Laser shadowgraphy was used to investigate the evolution of the critical plasma density region. Schlieren diagnostics were employed to image the plasma density gradients and to measure the plasma plume velocity and deceleration. Both shadow and schlieren diagnostics each allowed two frames per shot separated by 7 ns. The first shadow frame preceded the first schlieren frame by 2 ns. Both diagnostics systems used a 532 nm laser pulse with 120 mJ energy and 150 ps duration. The region probed in experiment is shown in Fig. 1A and B when viewed in the plane of the magnetic field, and in the plane perpendicular to the magnetic field, respectively.

Images obtained with these diagnostics are shown in Figs. 2 and 3. Early during the expansion the plasma pressure was much greater than the magnetic pressure and the ablation plume expanded hemi-spherically (Fig. 2A). As the plasma continued to expand, it was decelerated by the magnetic field, forming a discontinuity region with increased density (Fig. 2B). Shortly after the formation of the discontinuity, flute-like structures were observed (Fig. 2C). The structures were determined to be two-dimensional plasma sheaths since they were not observed in schlieren images taken in the plane of the magnetic field (Fig. 3).

Identifying the mechanism which leads to the formation of the flute-like structures and eventually to the plasma penetration through the magnetic field (Fig. 2D) requires knowledge of the plasma parameters. For the discontinuity region, several plasma parameters were determined from the laser diagnostics and others were estimated by using a resistive, radiation magnetohydrodynamics (MHD) code, as indicated in Table 1.

3 MHD modeling

A one-dimensional, two-temperature MHD simulation was performed using the Magneto-Hydro-Radiative-Dynamics Research (MHRDR) code (Lindemuth 1979) to determine the conditions present in the discontinuity region for times relevant to the onset of the growth of the flute-like structures. An Eulerian grid with cylindrical symmetry was used. The inital simulation geometry is shown in Fig. 4. The computational domain consisted of two regions, the laser target region, and the expansion region. The polyethylene target material was treated with an ideal gas equation of state.

In the target region, the simulation was initiated with polyethylene at solid state density (1000 kg/m^3) and both the electrons and ions at room temperature (0.026 eV). Based on hydrodynamic simulations with the code MULTI (Ramis et al. 1988), in the MHRDR simulation the laser energy was considered to be deposited in a 13 μm thick region adjacent to the expansion region. The electron temperature was considered to decrease linearly in the target bulk from a maximum value of 22 eV. The expansion region was modeled as initially containing a polyethylene gas with a density of 10^{-9} kg/m^3 corresponding to a residual pressure $p = 6 \times 10^{-6}$ Torr. The simulations included a magnetic

Table 1 Plasma parameters for the discontinuity region 10 ns after target ablation

Parameter name	Symbol	Value	Derived from
Scale length (mm)	L	0.2	Schlieren imaging
Velocity (m/s)	u	1×10^5	Schlieren imaging
Deceleration (m/s^2)	g	0.5–1 $\times 10^{13}$	Schlieren imaging
Perturbation wavelength (mm)	λ	0.2–0.4	Schlieren imaging
Magnetic field strength (T)	B	10–20	B-Dot measurements
Electron number density (cm^{-3})	n_e	0.5–1 $\times 10^{19}$	MHRDR simulations
Electron temperature (eV)	T_e	30–45	MHRDR simulations
Ion temperature (eV)	T_i	25–45	MHRDR simulations

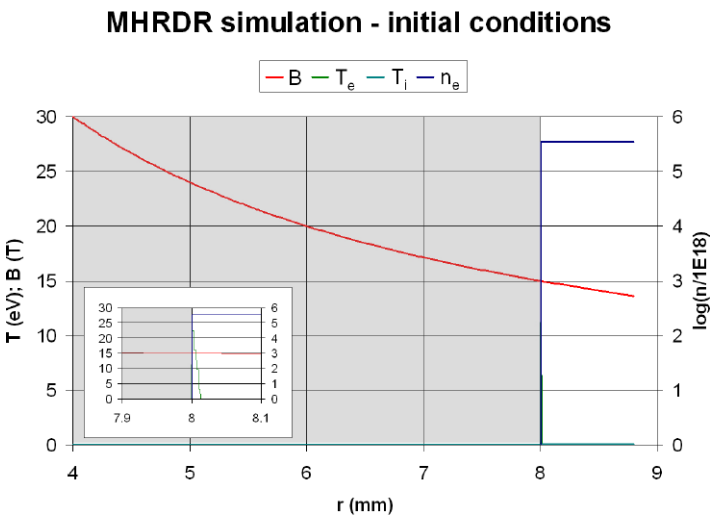

Fig. 4 Initial conditions used in the one-dimensional magnetohydrodynamic calculations with the code MHRDR. The *shaded area* indicates the expansion region and the non-shaded area the laser target region. The *inset* shows the initial electron temperature distribution in the heated region of the target

field with a $B \propto 1/r$ dependence, oriented perpendicular to the plane of calculation, and with a strength at the target surface in the range 10–20 T which included the experimental values.

As in experiment, in the simulation the heated region expanded and was decelerated by the magnetic field, forming a discontinuity region. An example of magnetic field, density and temperature distributions after 10 ns of expansion is shown in Fig. 5. The phase velocity of the critical density region in simulation matches that observed in experiment, as measured with shadow diagnostics. Additionally, the phase velocity of the discontinuity region in simulation matches the experimental value, measured by tracking the position of the high density gradient region with schlieren diagnostics. The MHRDR simulations were used to estimate the plasma density as well as the electron and ion temperature in the discontinuity region at the time the flute-like structures were observed in experiment (Fig. 2C). The parameters estimated with MHRDR are listed in Table 1 along with those measured in the experiment for the discontinuity region.

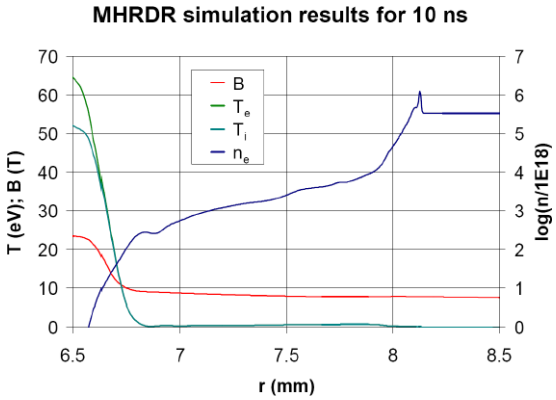

Fig. 5 Magnetic field, electron and ion temperature, and electron number density after 10 ns of expansion calculated with MHRDR for the initial conditions mentioned in the text

4 Results and discussion

The laser diagnostics indicated the formation of flute-like structures at the plasma—magnetic field interface, which ultimately allowed the plasma to penetrate the magnetic field (Figs. 2 and 3). The instability was initially seeded by imperfections in the laser beam profile or on the laser target surface. The instability can be classified using the growth

Table 2 Values of the coefficients in (4.2) and dimensionless plasma parameters estimated for the plasma parameter values given in Table 1. The magnetic Reynolds number is calculated using the Spitzer resistivity. β is the ratio between the plasma pressure and the magnetic pressure, $\rho_{i,d}$ is the ion gyroradius, and c/ω_{pi} is the ion collisionless skin depth. The solar wind parameters used: $n_i = n_e = 5 \times 10^6$ m^{-3}, $T_i = 10$ eV, $T_e = 20$ eV, $L = 1 \times 10^5$ m, $u = 4 \times 10^5$ m/s, and $B = 10$ nT

Coefficient	Experiment	Solar wind
Convective term	1	1
Diffusion term	1 ± 0.4	5×10^{-10}
Hall term	1 ± 0.5	0.25
Diagmagetic term	0.1 ± 0.05	0.05
Dimensionless plasma parameter	Experiment	Solar wind
β	0.5 ± 0.2	0.6
$\rho_{i,d}/L$	1.5 ± 0.2	1
$(c/\omega_{pi})/L$	0.8 ± 0.2	1

rate and wavelength. In experiment, $kL \sim 1$, where k is the wave number of the instability and L is the length scale of the discontinuity region. Using the plasma parameter values listed in Table 1, the growth rate was estimated for several instabilities which possess a flute-like structure that were likely to grow in the conditions present in the discontinuity region. For a highly conductive plasma, the magneto-Rayleigh-Taylor instability (MRTI, Kruskal and Schwarzschild 1954) would develop with an inverse growth rate of 3.6 ±1.5 ns. If the ion Larmor radius is larger than the characteristic size of the plasma, the large Larmor radius version of the Rayleigh-Taylor instability (LLRI, Hassam and Huba 1988) develops with an inverse growth rate of 4.5 ± 1.0 ns. Lastly, the electromagnetic flute instability (EMFI, Sotnikov et al. 2008) would grow with an inverse growth rate of approximately 10 ns.

Analysis indicates that the observations do not fit the EMFI and the LLRI characteristics. The EMFI is not likely responsible for the observed growth of the flute-like structures since nonuniformities of the boundary can be seen in experiment as early as 9 ns after the beginning of the plasma expansion. Moreover, the wave number k does not evolve in time, as is characteristic of the EMFI (Sotnikov et al. 2008). The LLRI requires a charge separation at the plasma-field interface, produced by unmagnetized ions. In experiment, the ion Larmor radius is comparable with the scale length (Table 2) and, in addition, the high collisionality prevents charge separation. Therefore the LLRI is an unlikely explanation of the observations, as well.

To understand how the remaining candidate, the MRTI, leads to plasma penetration across the magnetic field, a more detailed analysis of the plasma parameters in the discontinuity region is necessary. The time evolution of the magnetic field in the discontinuity region is described by the Faraday equation, using a form of Ohm's law appropriate for the conditions of the plasma investigated. For this experiment, Ohm's law is expressed as:

$$\boldsymbol{E} = -\boldsymbol{u} \times \boldsymbol{B} + \eta \boldsymbol{J} + \frac{1}{n_e e}(\boldsymbol{J} \times \boldsymbol{B} - \nabla P_e) \tag{4.1}$$

where e is the electron charge, η is the resistivity, n_e is the electron number density, P_e is the electron pressure (assumed to be isotropic), $\boldsymbol{u}$ is the plasma velocity, $\boldsymbol{J}$ is the current density vector, and $\boldsymbol{E}$ and $\boldsymbol{B}$ are the electric field and magnetic field vectors, respectively. On the right hand side (RHS) of (4.1), the first term is the convective term which appears in ideal MHD, the second term describes the diffusion of the magnetic field into the plasma, the third term accounts for the Hall effect, and the last term describes the plasma diamagnetism. The relative importance of these terms determines the characteristics of the field interaction with the plasma. Normalizing each of the terms on the RHS to the convective term $|\boldsymbol{u} \times \boldsymbol{B}|$, and using Ampère's law to eliminate $\boldsymbol{J}$ gives:

$$\boldsymbol{E} \approx |\boldsymbol{u} \times \boldsymbol{B}| \left(\hat{\boldsymbol{e}}_{convection} + \frac{1}{R_m} \hat{\boldsymbol{e}}_{diffusion} + Al \frac{c}{L\omega_{pi}} \hat{\boldsymbol{e}}_{Hall} + \frac{V_{e,th}}{V_A} \frac{\rho_{e,th}}{L} \hat{\boldsymbol{e}}_{diamagnetic} \right) \tag{4.2}$$

where ∇ is approximated with the inverse scale length $1/L$. The $\partial \boldsymbol{E}/\partial t$ term in Ampère's law is small for the plasma parameters given in Table 1 and was neglected. In (4.2) R_m is the magnetic Reynolds number, Al is the Alfvén number, ω_{pi} is the ion plasma frequency, $V_{e,th}$ is the electron thermal velocity, V_A is the Alfvén velocity, $\rho_{e,th}$ is the thermal electron gyroradius, and $\hat{\boldsymbol{e}}_{convection}$, $\hat{\boldsymbol{e}}_{diffusion}$, $\hat{\boldsymbol{e}}_{Hall}$, and $\hat{\boldsymbol{e}}_{diamagnetic}$, are unit vectors indicating the direction of the respective contributions.

The values of the dimensionless coefficients from the RHS of (4.2), calculated for the plasma parameters in the discontinuity region (Table 1), are listed in Table 2. The magnitude of each of the coefficients is of the order of 1, so none of the effects included can be neglected.

As the MRTI grows, the density and temperature in the expanding plasma flutes decrease. The magnetic field diffuses in the plasma with a characteristic time of about 2 ns. The expansion of the flutes causes collisions to become less frequent and the Hall effect to become more important. Eventually, charge separation becomes possible and the flute-like structures become polarized. The corresponding electric field is oriented perpendicular to both the magnetic field and the expansion velocity at the tip of the flutes. This effect enables the plasma flutes to penetrate the magnetic field by $\boldsymbol{E} \times \boldsymbol{B}$ drift, where $\boldsymbol{E}$ is the polarization field, and $\boldsymbol{B}$ is the magnetic field in the plasma.

In Table 2, the coefficients in the RHS of (4.2) for the experiment are compared with those for the solar wind in the region of the Earth's bow shock. For the case of the solar wind, only the Hall effect and the convection are significant. However, the solar wind is magnetized even in the absence of diffusion. The main improvement required for this experiment to become a pertinent laboratory simulation of the solar wind is reducing the plasma collisionality while maintaining its magnetization.

5 Conclusion

This paper presents an experiment in which a laser-produced plasma expands in an external magnetic field. In the absence of the field, the plasma expands hemispherically. When present, the magnetic field decelerates the front of the plasma plume, causing the perturbations present at the formation of the plasma plume to be amplified due to the magneto-Rayleigh-Taylor instability. As the instability grows, the perturbations develop into flute-like structures. The plasma flutes become polarized and are able to penetrate the field due to $\boldsymbol{E} \times \boldsymbol{B}$ drift.

Acknowledgements The authors of this paper would like to acknowledge Vladimir Ivanov, Alexey Morozov, Mike Bakeman, Gary Pettee, and Alexey Astanovitskiy. This work was supported by DOE/NNSA grant DE-FC52-06NA27616.

References

Axford, W.I., Hines, C.O.: A unifying theory of high-latitude geophysical phenomena and geomagnetic storms. Can. J. Phys. **39**(10), 1433–1464 (1961)

Dungey, J.W.: Interplanetary magnetic field and the auroral zones. Phys. Rev. Lett. **6**(2), 47–48 (1961)

Echim, M.M., Lemaire, J.F.: Laboratory and numerical simulations of the impulsive penetration mechanism. Space Sci. Rev. **92**(3), 565–601 (2000)

Gratton, F.T., Farrugia, C.J., Cowley, S.W.H.: Is the magnetopause Rayleigh-Taylor unstable sometimes? J. Geophys. Res. **101**(A3) (1996)

Hassam, A.B., Huba, J.D.: Magnetohydrodynamic equations for systems with large Larmor radius. Phys. Fluids **31**, 318 (1988)

Kruskal, M., Schwarzschild, M.: Some instabilities of a completely ionized plasma. Proc. R. Soc. Lond., Ser. A, Math. Phys. Sci. **223**(1154), 348–360 (1954) (1934–1990)

Lindemuth, I.: The ANIMAL code. Lawrence Livermore National Laboratory Report, ucrl-52492 edition (1979)

Ramis, R., Schmalz, R., Meyer-Ter-Vehn, J.: MULTI—A computer code for one-dimensional multigroup radiation hydrodynamics. Comput. Phys. Commun. **49**, 475–505 (1988)

Sotnikov, V.I., et al.: Investigation of compressible electromagnetic flute mode instability in finite beta plasma in support of z-pinch and laboratory astrophysics experiments. Commun. Comput. Phys. **4**, 611 (2008)